Pergamon

Neuroscience Vol. 92, No. 2, pp. 427–443, 1999

PII: S0306-4522(99)00024-X
0306-4522/99 $20.00+0.00

CORTICALLY-INDUCED COHERENCE OF A THALAMIC-GENERATED OSCILLATION

A. DESTEXHE,* D. CONTRERAS† and M. STERIADE

Laboratoire de Neurophysiologie, Faculté de Médecine, Université Laval, Québec, Canada, G1K 7P4

Abstract—Oscillatory patterns in neocortical electrical activity show various degrees of large-scale synchrony depending on experimental conditions, but the exact mechanisms underlying these variations of coherence are not known. Analysis of multisite local field potentials revealed that the coherence of spindle oscillations varied during different states. During natural sleep, the coherence was remarkably high over cortical distances of several millimeters, but could be disrupted by artificial cortical depression, similar to the effect of barbiturates. Possible mechanisms for these variations of coherence were investigated by computational models of interacting cortical and thalamic neurons, including their intrinsic firing patterns and various synaptic receptors present in the circuitry. The model indicates that modulation of the excitability of the cortex can affect spatiotemporal coherence with no change in the thalamus. The highest level of coherence was obtained by enhancing the excitability of cortical pyramidal cells, simulating the action of neuromodulators such as acetylcholine and noradrenaline. The underlying mechanism was due to cortex–thalamus–cortex loops in which a more excitable cortical network generated a more powerful and coherent feedback onto the thalamus, resulting in highly coherent oscillations, similar to the properties measured during natural sleep.

In conclusion, these experiments and models are compatible with a powerful role for the cortex in triggering and synchronizing oscillations generated in the thalamus, through corticothalamic feedback projections. The model suggests that intracortical mechanisms may be responsible for synchronizing oscillations over cortical distances of several millimeters through cortex–thalamus–cortex loops, thus providing a possible cellular mechanism to explain the genesis of large-scale coherent oscillations in the thalamocortical system. © 1999 IBRO. Published by Elsevier Science Ltd.

Key words: sleep, spindle, coherence, computational models, neuromodulation, spatiotemporal.

Sleep spindle oscillations have been investigated thoroughly during the last decades. One of the reasons for the success of this investigation is the fact that spindles are exacerbated by some anesthetics, such as barbiturates, which greatly facilitates recordings of these oscillations *in vivo*.[3,47] Further, the discovery of an *in vitro* model of spindles in ferret thalamic slices[55] enabled in-depth pharmacological investigation and biophysical characterization. The design of detailed computational models helped to test possible cellular mechanisms to generate these oscillations (reviewed in Ref. 18), based on the complex cellular firing properties and the multiple types of synaptic receptors present in thalamic circuits.

To account for the large-scale synchrony and distribution of these oscillations in the neocortex, Andersen and Andersson[3] proposed a model in which different oscillating sites in the thalamus were linked by "distributor" cells, which would connect thalamocortical (TC) cells by intrathalamic excitatory axon collaterals. No evidence was yet obtained for such neurons. More recently, multielectrode thalamic recordings have shown that the large-scale synchrony of oscillations is lost in the thalamus following decortication,[13] which rules out intrathalamic synchronizing mechanisms based on connections between dorsal thalamic nuclei. Still, epochs characterized by clear-cut synchronization of spindles persisted in the thalamus deprived from cortex, possibly due to connections involving the thalamic reticular (RE) nucleus.[14]

In a recent computational model of these oscillations,[19] it was suggested that the large-scale synchrony can be explained by mutual interactions between cortex and thalamus. According to this mechanism, the synchrony depends mainly on corticothalamic feedback on RE cells, with a more limited role for intrathalamic synchronizing mechanisms. This model also accounted for different properties of barbiturate spindles, such as their waxing-and-waning envelope, their refractory period and their relatively high variability.

However, a series of points still remain unclear.

*To whom correspondence should be addressed.
†Present address: Department of Neuroscience, University of Pennsylvania School of Medicine, Philadelphia, PA 19104, U.S.A.

Abbreviations: AMPA, α-amino-3-hydroxy-5-methyl-4-isoxazolepropionic acid; EEG, electroencephalogram; EPSP, excitatory postsynaptic potential; IN, cortical interneuron; IPSP, inhibitory postsynaptic potential; LFP, local field potential; PY, cortical pyramidal cell; RE, thalamic reticular cells; TC, thalamocortical cells.

First, corticocortical connections have negligible role in the large-scale synchrony of barbiturate spindles,[13,14] but the interhemispheric synchrony is reduced in cats following section of the corpus callosum,[7] suggesting that at least some intracortical connections are important. Second, during natural sleep, spindle oscillations are often characterized by a strict simultaneity (see Fig. 1 in Ref. 14) by contrast to barbiturate anesthesia which show high variability (see Fig. 7 in Ref. 3; see also Ref. 12). This suggests that the patterns of large-scale synchrony may be significantly different between these states, but no detailed investigation of this aspect is at present available.

In this paper, we re-examined, quantified and compared the large-scale synchrony of spindle oscillations during three states: natural sleep, natural sleep following artificial depression of the cortex, and barbiturate anesthesia. With computational models, we investigated possible mechanisms to explain the different levels of large-scale synchrony found in natural sleep, depressed cortex and anesthetized conditions. We investigated the hypothesis that coherence can be modulated by purely intracortical mechanisms without the involvement of intrathalamic synchronizing mechanisms.

EXPERIMENTAL PROCEDURES

Multisite recordings

Multisite local field potentials (LFPs) were recorded from the suprasylvian gyrus of anesthetized ($n = 7$) and chronically-implanted naturally-sleeping adult cats ($n = 3$; animals were provided by the Service des Animaux de Laboratoire, Université Laval, Québec, Canada). The electrode location is illustrated in the top scheme of Fig. 1. All efforts were made to minimize animal suffering and reduce the number of animals used. Experimental procedures were described in detail elsewhere.[12,14]

In two of the experiments on naturally-sleeping animals, cortical depression was induced by releasing a drop of highly concentrated potassium acetate (3 M) in the vicinity of electrode 1. This experimental procedure has been detailed previously.[12] The potassium solution induced a complete flattening of the LFPs. After a period of a few seconds of complete absence of cortical activity, spindle waves gradually re-appeared and were analysed before the cortex recovered normal activity (about 60 s).

Data analysis

The spatiotemporal coherence of spindle oscillations was quantified by computing spatiotemporal maps of the distribution of electrical activity across the cortex, the distribution of initiation times and the decay of correlations with distance.

Spatiotemporal maps of activity were constructed as follows. A snapshot of the distribution of electrical activity across the cortex was generated by assigning a color spot to the instantaneous value of LFP at each electrode and arranging color spots along a horizontal line (anterior-to-posterior axis). Only negative deflections of LFPs were converted to color (typically from 0 to -150 μV). Successive snapshots were arranged vertically in columns, defining a map where LFP is represented as a function of space and time. Synchronous events therefore appear as horizontal straight lines, while oblique lines stand for propagating waves or phase shifts.

Initiation times were computed to quantify the simultaneity of spindle sequences and estimate the spatiotemporal pattern of initiation. The initiation of the oscillation in one site was estimated as the first negativity–positivity complex that exceeded 25% of the total deflection of amplitude of the subsequent spindle. This estimation was performed for each site and the respective times of first negativity–positivity were plotted as a function of distance or electrode number. Several spindle waves were processed using this procedure and the data were grouped in the same graph (Fig. 1B). This graph was also used to compute the distribution of initiation times (see Fig. 1C). This distribution estimates the "time jitter" of initiation, which was quantified by computing the standard deviation (σ) of the distribution.

The spatial coherence was evaluated by computing the spatial correlation:

$$C(x) = \frac{\Sigma_{i,j} v\left(r_i, t_j\right) v\left(r_i + x, t_j\right)}{\Sigma_{i,j} v\left(r_i, t_j\right)^2} \qquad (1)$$

where $v(r_i,t_j)$ is the normalized LFP at site r_i and time t_j. Signals were normalized by subtraction of their average value and division by their standard deviation. Cross-correlations were then calculated between every possible pair of renormalized signals and the values at time zero were combined for all pairs with same intersite distance (x). The same procedure was repeated for several epochs of spindle activity and averaged together. The representation of the averaged correlation as a function of distance was used to measure the decay of correlation with distance in the anterior–posterior axis of the suprasylvian cortex.

As the decay of spatial correlations was always smooth towards zero, a first-order decaying exponential term was used to fit the correlation data:

$$C(x) = \exp(-x/\lambda) \qquad (2)$$

where the space constant, λ, is a measure of the spatial extent of the coherence of a spatially homogeneous phenomenon, similar to the coherence measure based on power spectra.[8] A closely related—but different—measure of spatial coherence is by representing the peak of the cross-correlation as a function of distance. Using either procedures yielded no appreciable difference for the signals studied here because cross-correlations peaked at time zero.

Computational models

Layer VI pyramidal neurons constitute the major source of corticothalamic fibers and these cells receive a significant proportion of their excitatory synapses directly from the thalamus, therefore mediating a monosynaptic excitatory feedback loop (thalamus–cortex–thalamus).[25,57] This monosynaptic bidirectional interaction between thalamus and cortical layer VI was modeled by a four-layer thalamocortical network with the following cell types: cortical pyramidal cells (PY), cortical interneurons (IN), RE and TC cells. The cellular models were single-compartments containing intrinsic and synaptic currents, and were identical to a model introduced previously.[19]

Every cell was described by the membrane equation:

$$C_m \dot{V}_i = -g_L(V_i - E_L) - \sum_j I_{ji}^{int} - \sum_k I_{ki}^{syn} \qquad (3)$$

where V_i is the membrane potential, $C_m = 1$ $\mu F/cm^2$ is the specific capacity of the membrane, g_L is the leakage conductance and E_L is the leakage reversal potential. Intrinsic and synaptic currents are, respectively, represented by I_{ji}^{int} and I_{ki}^{syn}.

Intrinsic currents were modeled using kinetic models of

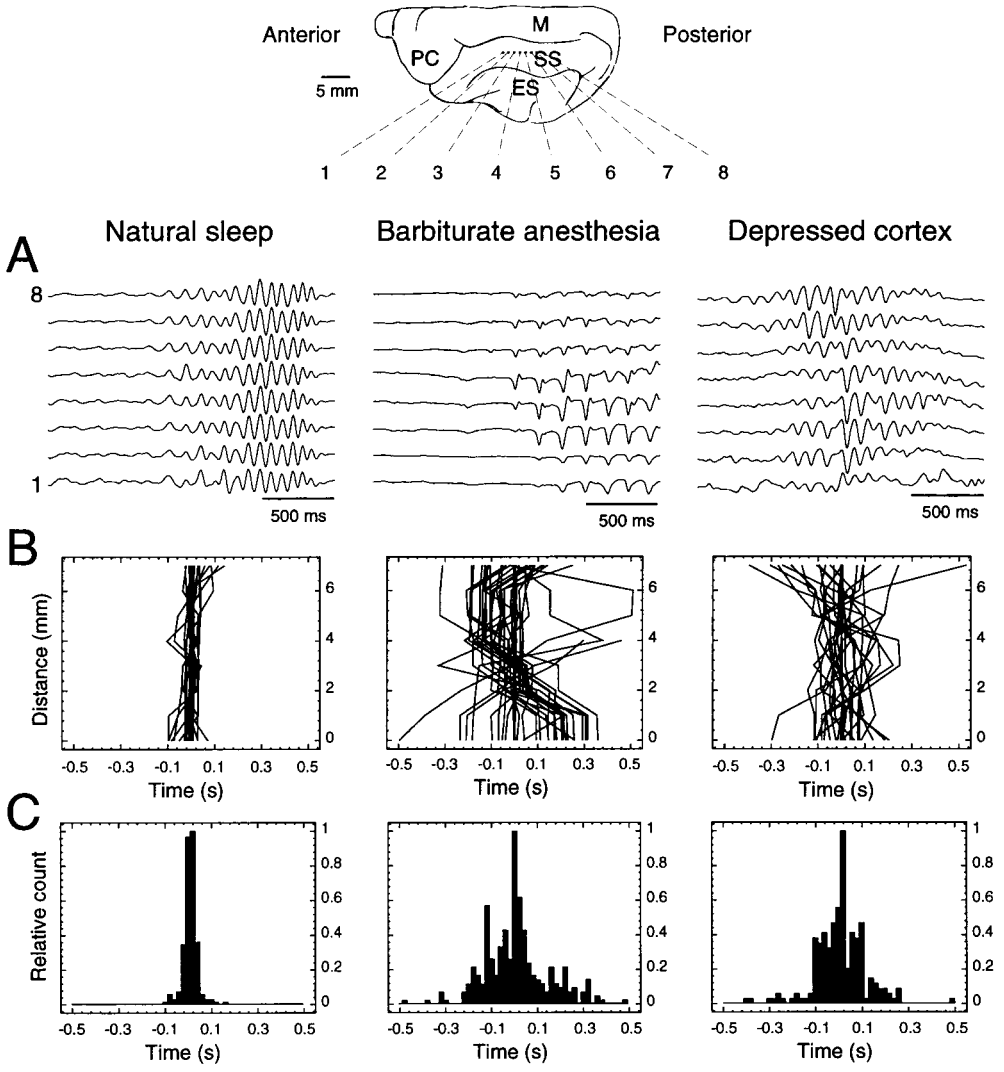

Fig. 1. Spatiotemporal distribution of spindle oscillations in cat cerebral cortex. The top scheme indicates the localization of electrodes in area 5–7 of cat cortex (ES, ectosylvian gyrus; M, marginal gyrus; PC, postcruciate gyrus; SS, suprasylvian gyrus). The three panels from left to right indicate recordings in naturally-sleeping animals (Natural sleep), in anesthetized animals (Barbiturate anesthesia), and in natural sleep following cortical depression (Depressed cortex). (A) Multisite field potentials during spindle oscillations. The local field potentials recorded simultaneously in different sites are shown for three representative spindle sequences. (B) Initiation patterns of spindle oscillations. The time of initiation of the oscillation was detected for each site (see Experimental Procedures). The relative initiation times were drawn as a line (vertical line = simultaneous), with one different line for each spindle sequence. (C) Distribution of initiation times computed from the graphs in B.

the Hodgkin and Huxley[27] type. All models had Na^+ and K^+ currents for generating action potentials, which kinetics was taken from a previous study.[52] Additional currents conferred to the cells the most salient features of thalamic and cortical intrinsic firing patterns (summarized in Fig. 3B). Thalamic cells produced bursts of action potentials due to the presence of a T-current. In TC cells, in addition to I_T, the presence of I_h conferred oscillatory properties. The upregulation of I_h by intracellular Ca^{2+} led to waxing-and-waning properties of these oscillations, as detailed in previous models.[21,22] In RE cells, the T-current was of slower kinetics[28] as described in a previous model.[23] Models for cortical cells were kept as simple as possible. Interneurons contained no other current than action potential, producing similar firing patterns as "fast spiking" cells.[10] Pyramidal cells had one additional voltage-dependent K^+ current responsible for spike adaptation (I_M). Due to the presence of this current, cortical PY cells generated adapting trains of action potentials, similar to "regular spiking" pyramidal cells.[10]

Synaptic currents were described by kinetic models of postsynaptic receptors. When a spike occurred in the presynaptic cell, a brief pulse of transmitter (0.5 mM during 0.3 ms) was delivered to receptors that followed a simple open/closed kinetic scheme, leading to a transient increase of postsynaptic current. This simple scheme can account for the time-course of most fast types of synaptic interaction.[20] The modeling of slow $GABA_B$ receptor-mediated inhibition required a more complex scheme to capture the nonlinear properties of this type of interaction.[20] The parameters of all models for synaptic currents were adjusted to experimental recordings using simplex fitting methods.[20] The effect of barbiturates in slowing down $GABA_A$ currents [51] was also taken into account (see details in Ref. 19).

The pattern of connectivity between the different cell

types is schematized in Fig. 3A. The thalamic network was identical to a previous model[22] with TC and RE cells reciprocally connected using α-amino-3-hydroxy-5-methyl-4-isoxazolepropionic acid (AMPA) type of synaptic receptor (TC → RE) and $GABA_A$ and $GABA_B$ receptors (RE → TC) while RE cells inhibit each other via $GABA_A$ receptors. Cortical cells were also reciprocally connected with AMPA receptors (PY → PY and PY → IN) and a mixture of $GABA_A$ and $GABA_B$ receptors (IN → PY). Thalamocortical (TC → PY and TC → IN) and corticothalamic (PY → TC and PY → RE) projections were mediated by AMPA receptors. No qualitative effect was observed when *N*-methyl-d-aspartate receptors were added to all excitatory connections (25% of maximal conductance of AMPA receptors) and were therefore not included.

The thalamocortical network was organized in four one-dimensional layers with 100 cells of each type; each layer made connections with other layers (Fig. 3A). The intrinsic connectivity in the thalamus and the cortex was topographic and the axonal projections extended over 11 cells, similarly to a previous study of thalamic networks.[22] Projections between thalamus and cortex were also topographic, but more divergent, consistent with anatomical studies.[29,33,40] The anatomical bases underlying this type of connectivity were detailed in previous papers.[19,22]

In a previous study,[19] it was shown that calculating average membrane potentials using an intersite distance of 11 cells led to similar propagation velocity as in experiments, suggesting that this distance roughly corresponds to the interelectrode distance of 1 mm in the experimental setup. The network of 100 cells therefore represents about 9 mm of cerebral cortex and each cortical cell represents a volume of about 90 μm diameter in cortex (1 mm/11), which represents about 315 cortical neurons (assuming a density of 100,000 neurons/mm^3).

All cells of each type received an identical pattern of synaptic connections and had identical intrinsic properties, with the exception of TC cells. I_h conductance values were randomly distributed among TC cells across the network such that several TC cells were spontaneous oscillators[19] and served as initiation sites from where the oscillation spread to the whole network. In these conditions, the network generated spindle oscillations with similar cellular discharge patterns as in experiments and was robust to change in parameters.[19]

The effect of cortical excitability was integrated into model pyramidal cells as follows. First, the resting membrane potential was set to a more depolarized value in cortical PY cells (−60 mV instead of −70 mV), mimicking the effect of several neuromodulators in closing leak K^+ currents.[35] Second, the I_M conductance responsible for adaptation in cortical PY cells was reduced (from 0.07 mS/cm^2 to 0.02 mS/cm^2), to mimic the effect of acetylcholine, noradrenaline and metabotropic glutamate receptor agonists.[56] These two actions resulted in resting membrane potentials of PY cells closer to *in vivo* recordings during light barbiturate anesthesia (between −60 and −70 mV). All other parameters remained constant in order to investigate specifically the effect of increasing the excitability of cortical pyramidal cells.

The effect of enhancing excitability was also tested for other cell types in the network. In IN cells, the resting level was varied from −90 to −60 mV. In thalamic cells, the leak K^+ current was decreased by 2 nS (TC cells) and the leak conductance was reduced to 40% of its control value (RE cells). These changes led to increased excitability because of a larger input resistance and/or more depolarized resting levels. These effects are similar to the action of several neuromodulators such as noradrenaline and serotonin,[35] although the effects on voltage-dependent currents were not included for simplicity.

Simulations were done using NEURON[26] and analyses were performed using C programs based on a library of numerical algorithms.[39] All simulations and analyses were run on a Sparc 20 workstation (Sun Microsystems, Mountain View, CA).

RESULTS

Analysis of experimental data is shown first, to illustrate that the spatiotemporal coherence of the same type of oscillations can differ for different states of the cortex. Then, a computational model is introduced to test the hypothesis that the state of excitability of the cortex can control the coherence of oscillations, with no need for specific intrathalamic mechanisms.

Spatiotemporal coherence of spindle oscillations

During natural sleep, electroencephalogram (EEG) recordings in humans and LFPs in the suprasylvian cortex of cats revealed that spontaneous spindles appear coherently over distances up to 15 mm.[14] Spindle sequences were analysed from three naturally-sleeping cats ($n = 24$) at the onset of slow-wave sleep. An array of eight equidistant extracellular electrodes was used to record simultaneously in different sites of the cortex (see scheme in Fig. 1). Sleep spindle oscillations appeared with a remarkable synchrony among the eight electrodes (Fig. 1A, Natural sleep).

The relative initiation times of the oscillation at each electrode were calculated from multisite LFPs (see Experimental Procedures) and are illustrated in Fig. 1B (Natural sleep). Spindle sequences ($n = 24$) analysed from naturally sleeping cats initiated within time windows of the order of 0.05 ± 0.03 s (mean ± S.D.), corresponding to an average velocity of 140 mm/s. The distribution of initiation times (Fig. 1C, Natural sleep) was relatively narrow and had a standard deviation of $\sigma = 31$ ms.

During barbiturate anesthesia, similar to the early phase of slow-wave sleep, the activity of the cortex is dominated by spindle oscillations. These oscillations are of slower frequency than natural sleep spindles (6–8 Hz vs 10–12 Hz), but they have the same cellular correlates.[47,48] They are also known to be highly coherent over the cortical hemisphere.[3] However, at closer scrutiny, it appeared that barbiturate spindles initiate in looser time windows compared to natural sleep (Fig. 1A). Measuring the initiation times of these oscillations ($n = 35$; Fig. 1B, Barbiturate anesthesia) led to time windows of about 0.20 ± 0.13 s (average velocity of 35 mm/s). Figure 1B also shows that, not only the initiation time is loose, but there is considerable variability in the number of initiation sites, their relative timing and their location from one sequence to the next. The distribution of initiation times (Fig. 1C, Barbiturate anesthesia) was broad (standard deviation of $\sigma = 139$ ms).

The highly coherent patterns of natural sleep spindles can be disrupted by artificial depression of

the cortex.[12] During the recovery period following cortical depression induced by potassium acetate in natural sleep, spindles appear as the first sign of activity. Spindle waves recorded at that time, before the cortex had completely recovered, were analysed and are shown in Fig. 1A (Depressed cortex). The depression of the cortex during natural sleep led to similar patterns of initiation of spindles as during barbiturate anesthesia (Fig. 1A).

Measuring initiation times in two cats ($n = 27$), during the recovery period of spreading depression (Fig. 1B, Depressed cortex), showed that oscillations initiated within time windows of 0.18 ± 0.11 s (average velocity of 39 mm/s). Similar to barbiturate anesthesia, there was considerable variability in the number, location and timing of initiation sites (Fig. 1B). After complete recovery from cortical depression, the synchrony of spindles came back to that of natural sleep in control conditions[12] and so did their patterns of initiation (not shown). The distribution of initiation times (Fig. 1C, Depressed cortex) was similar to that obtained during barbiturate anesthesia (standard deviation of $\sigma = 108$ ms).

A decrease in spatiotemporal coherence during anesthesia and cortical depression was apparent in the spatiotemporal distribution of activity across the cortex. Spatiotemporal maps were constructed by representing LFP negativity as a function of distance and time (Fig. 2, top panels). During natural sleep, oscillatory activity began almost simultaneously over all electrodes (Fig. 2, Natural sleep). The oscillations were synchronized, as indicated by the formation of yellow (maximum local activity) and blue (local silence) stripes at 10–12 Hz. Barbiturate spindles occurred at lower frequency (6–8 Hz) and were less organized than natural sleep (Fig. 2, Barbiturate). The oscillation began simultaneously at one or several sites and subsequently invaded the rest of the recorded area. The first spindle illustrated in the middle-top panel of Fig. 2 shows two initiation sites, while the other ones show a single site for initiation. The last column shows a local oscillation that did not invade the network. Blue–yellow stripes were not perfectly horizontal, which indicates the existence of phase shifts among the cortical sites. Cortical depression drastically reduced the spatiotemporal coherence of natural sleep spindles, as shown by the more disorganized pattern of activity (Fig. 2, Depressed cortex), similar to barbiturate anesthesia.

The spatiotemporal coherence was characterized by evaluating the decay of correlations with distance in the cortex (Fig. 2, bottom panels), for distances of 0 to 7 mm in steps of 1 mm as determined by the configuration of the recording electrodes. During natural sleep, correlations showed a limited decay with distance, showing values above 0.75 for distances up to 7 mm. The space constant was $\lambda = 25$ mm (see Experimental Procedures). During barbiturate anesthesia or following cortical depression, spatial correlations had a more marked decay with distance. In this case, spatial correlation attained values around 0.3–0.4 for distances up to 7 mm and the space constant was of $\lambda = 5.4$ mm and $\lambda = 6.5$ mm, respectively. When comparing natural sleep to barbiturate or depressed cortex, the space constant was reduced four to five times, similar to the difference in initiation times (see above).

This analysis shows that sleep spindle oscillations appear highly synchronously, almost simultaneously over cortical distances of several millimeters. On the other hand, during anesthesia or following cortical depression, the same oscillations are less coherent. A possible mechanism to account for these observations is investigated below.

Computational models of cortical excitability

As spindle oscillations are generated in the thalamus, an immediate suggestion would be that different states of coherence of these oscillations correspond to different states in the thalamic circuitry. However, the decreased coherence following cortical depression indicates that this is not a consequence of intrathalamic mechanisms alone. We suggest here that this difference is due to the influence of the cortex on the thalamus via corticothalamic feedback. This is supported by experiments showing the decisive effect of corticothalamic feedback on intrathalamic coherence.[13] The main hypothesis explored below is that differences in coherence of thalamic-generated oscillations are due to different levels of cortical excitability.

It is known that the excitability of cortical pyramidal cells is regulated by a number of factors. First, the excitability of the cortical network is considerably higher during the awake state. Ascending activating systems from brain stem, basal forebrain and posterior hypothalamus release neuromodulatory substances such as acetylcholine, noradrenaline, serotonin and histamine in cortex and thalamus.[43] Stimulation of these regions results in a marked depolarization of intracellularly recorded pyramidal cells[44] and a subsequent increase in excitability. Second, extracellular application of neuromodulatory substances in cortical slices induces a depolarization of cortical pyramidal neurons and increase of their excitability.[36–38] For instance, it was shown that subthreshold stimuli can become suprathreshold in the presence of acetylcholine.[36] Third, neuromodulators such as acetylcholine and noradrenaline act on pyramidal cells via diminution of the conductances responsible for adaptation of firing and closing of leak K^+ currents.[32,35,56]

In this model, cortical excitability was incorporated through effects on pyramidal cells mainly. In control conditions, the resting membrane potential of cortical pyramidal cells was around -70 mV and the spike frequency adaptation was important (Fig. 3B). This behavior was similar to pyramidal cells recorded *in vitro*[10,11] and *in vivo* during barbiturate

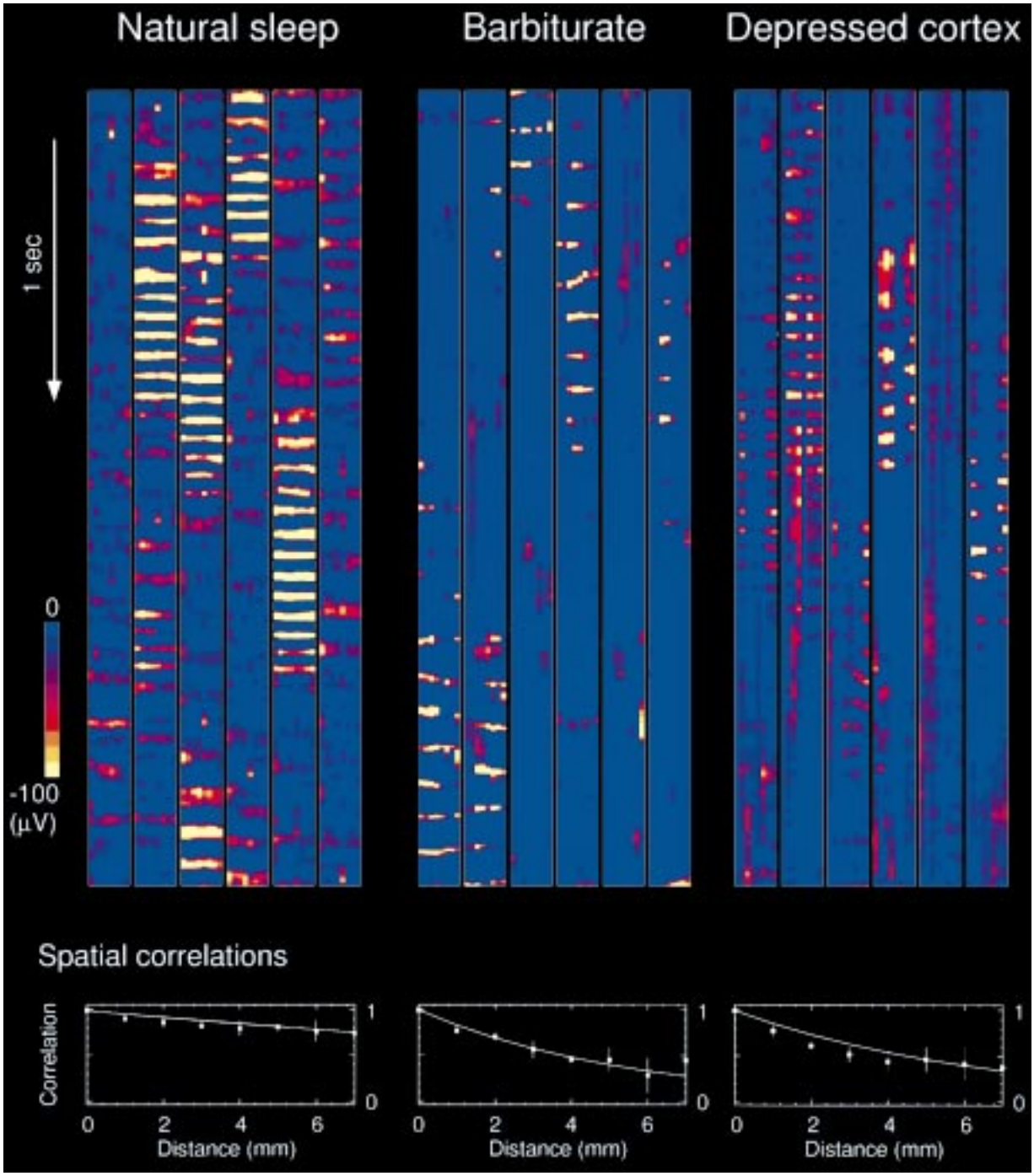

Fig. 2. Diminished spatiotemporal coherence of spindle oscillations during anesthesia and cortical depression. (Top panels) Spatiotemporal maps of the distribution of electrical activity across the cortex were constructed by assigning a color to the value of the field potential at each electrode; the color scale ranged in 10 steps from the baseline (blue) to −100 μV (yellow). Time was divided in frames each representing a snapshot of 4 ms of cortical activity and arranged in columns from top to bottom. A total of about 18 s of activity (4560 frames) is shown in six columns (arrow is one second). Each frame consisted of eight color spots, each corresponding to the LFP of one electrode from anterior to posterior (left to right in each column). (Bottom panels) Decay of correlations with distance. Cross-correlations were computed for all possible pairs of sites and the value at time zero was represented as a function of the intersite distance in the cortex. Each point is an average over different combination of sites, and 10 different epochs of 2 s; vertical bars indicate the standard deviation. Continuous lines indicate the best fit using a decaying exponential.

anesthesia.[49] A state of enhanced excitability was simulated in pyramidal cells by reducing the I_M conductance, leading to less prominent spike frequency adaptation (Fig. 3B, Enhanced excitability),

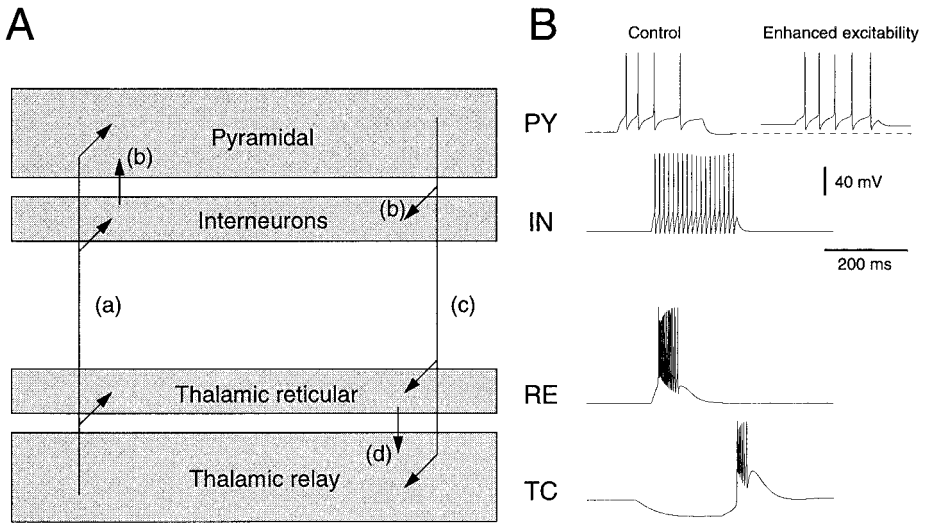

Fig. 3. Connectivity and firing patterns of thalamic and cortical cells in the model. (A) Diagram indicating the connectivity between the different cell types. Synaptic connections were simulated by kinetic models of post-synaptic receptors (AMPA receptors for excitatory connections and a mixture of $GABA_A$ and $GABA_B$ receptors for inhibitory connections; see Experimental Procedures). Thalamocortical (TC) relay cells do not connect to each other but project to all other cell types in the network (a). Cortical pyramidal (PY) cells and interneurons (IN) form a network with local connectivity (b). PY cells contact all cell types in the network (c). Thalamic reticular (RE) cells form an inhibitory network and project to TC cells (d). (B) Intrinsic firing patterns were simulated using models of the Hodgkin–Huxley type. The intrinsic firing patterns were: regular-spiking PY cell (depolarizing pulse of 0.75 nA during 200 ms; −70 mV rest), fast spiking IN (same pulse), bursting RE cell (pulse of 0.3 nA during 10 ms) and rebound burst in a TC cell (pulse of − 0.1 nA during 200 ms). The response of the cortical PY cell is shown in control conditions and with enhanced excitability (reduced I_M and more depolarized rest; see Experimental Procedures).

similar to intracellularly-recorded neocortical neurons in awake cats.[6] The resting membrane potential was also more depolarized, around −60 mV, as reported from intracellular studies in awake cats.[6]

To investigate the effect of enhancing pyramidal cell excitability at the network level, a one-dimensional network was constructed with 50 cortical pyramidal cells (PY) with spike frequency adaptation and 50 cortical interneurons (IN) with no frequency adaptation (cells shown in Fig. 3B). Excitatory interactions (PY → PY and PY → IN) were mediated by AMPA receptors while inhibitory interactions (IN → PY) were mediated by a mixture of $GABA_A$ and $GABA_B$ receptors. Connections were local, with each cell type contacting the 11 closest neighbors for each type of connection.

In control conditions, with all cortical cells having a resting level of −70 mV, an initial discharge did not propagate beyond the stimulation site (Fig. 4A1). This is consistent with experiments in cortical slices that show a very limited horizontal propagation of discharges in normal conditions.[9] This limited spatial propagation can also be seen from spatiotemporal maps of the distribution of electrical activity across the network (Fig. 4B, −70 mV). The initial stimulus evoked excitatory postsynaptic potentials (EPSPs) in neighboring PY cells, but did not evoke spikes.

A radically different behavior was seen when the excitability of pyramidal cells was enhanced. Figure 4A2 shows the same simulation as in Fig. 4A1 with more depolarized rest and decreased I_M conductance in PY cells. In these conditions, the previously subthreshold EPSPs became suprathreshold and led to the propagation of discharges across the network. The same phenomenon is shown in Fig. 4B for different values of the resting membrane potential. With resting levels of −67 and −63 mV, the initial discharge led to spiking of neighboring cells, but the discharge did not propagate further. With −60 and −55 mV rest, the initial discharge propagated across the network. The propagation velocity was fast, with a velocity of about 100–200 mm/s assuming the distance correspondence of 11 cells for 1 mm (see Experimental Procedures). The velocity was proportional to the difference between the resting level and action potential threshold (not shown). At −55 mV, the cell was resting just below action potential threshold and in this case, the propagation velocity was maximal.

These simulations show that, for this parameter range, the resting potential of pyramidal cells is critical to determine the extent of spread of discharges across the network. Simulations realized for other sets of parameters, including different values of excitatory and inhibitory conductances, led to similar results (not shown). The critical value of the resting level to allow fast-propagating discharges

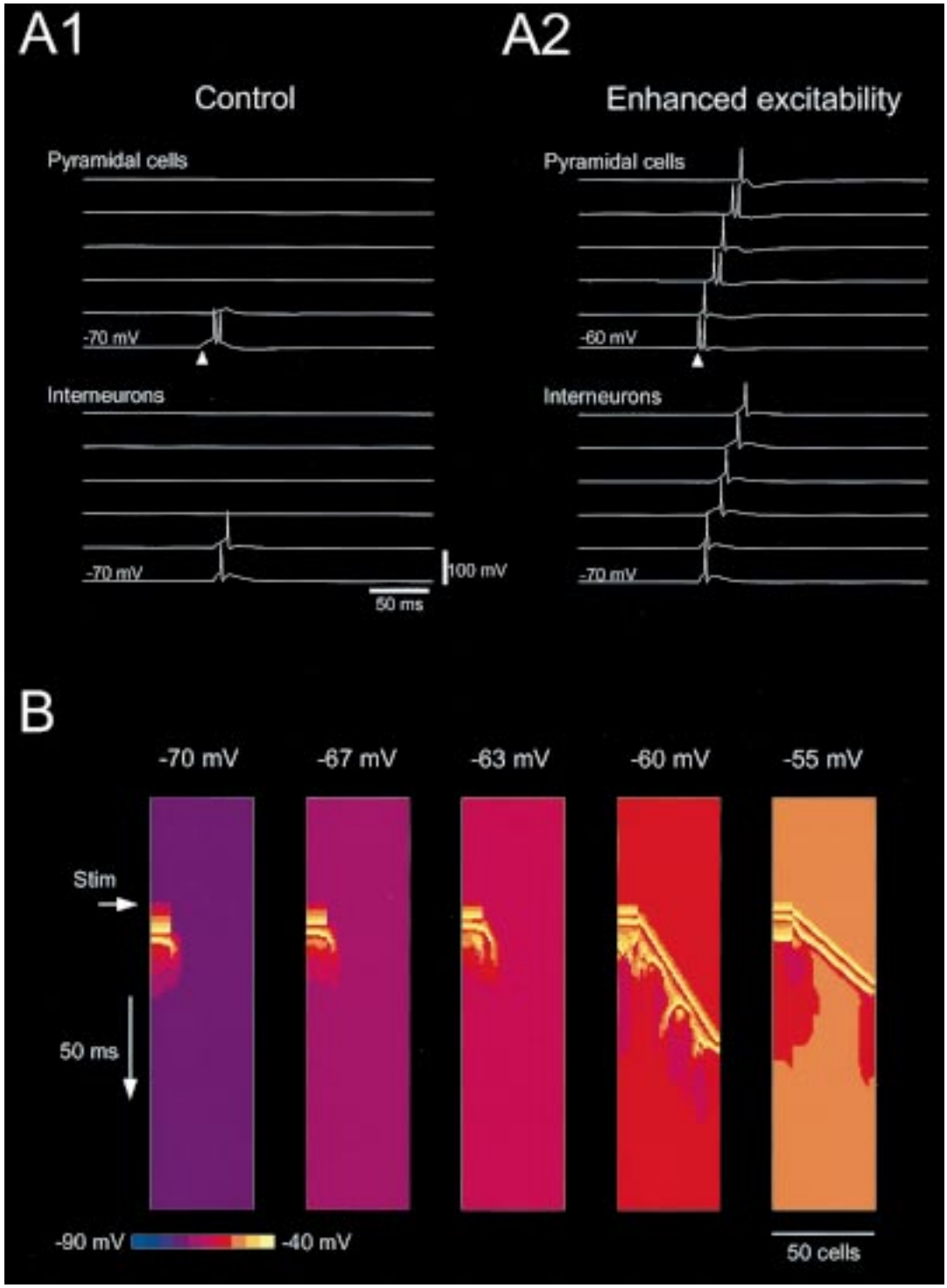

Fig. 4. Fast-propagating discharges in a network of cortical pyramidal cells and inhibitory interneurons. 50 pyramidal cells and 50 interneurons were simulated. The first 10 cells were fired by injecting a depolarizing current pulse (arrow; pulse of 1 nA during 20 ms). (A) Cellular patterns of discharge. A simulation in control conditions (A1; all cells resting at −70 mV; I_M conductance of 0.07 mS/cm^2) is compared to the same simulation with enhanced excitability of cortical pyramidal cells (A2; −60 mV rest for PY cells; I_M conductance reduced to 0.02 mS/cm^2). Cells 1, 11, 21, 31, 41 and 50 are shown for each type. (B) Spatial patterns of discharge. The same simulation as in A was performed, but the resting level of PY cells was varied from −70 to −55 mV (I_M conductance of 0.07 mS/cm^2 for −70 mV and 0.02 mS/cm^2 for all other cases). For each case, a spatiotemporal map of the distribution of electrical activity is shown, where the membrane potential of PY cells is shown in the horizontal axis, while the vertical axis represents time (from top to bottom; calibration arrow indicates 50 ms). The voltage was coded using the grey-scale shown below. Synaptic conductances were 0.6 μS (PY→PY AMPA receptors), 0.2 μS (PY→IN AMPA receptors), 0.15 μS (IN→PY $GABA_A$ receptors) and 0.03 μS (IN→PY $GABA_B$ receptors).

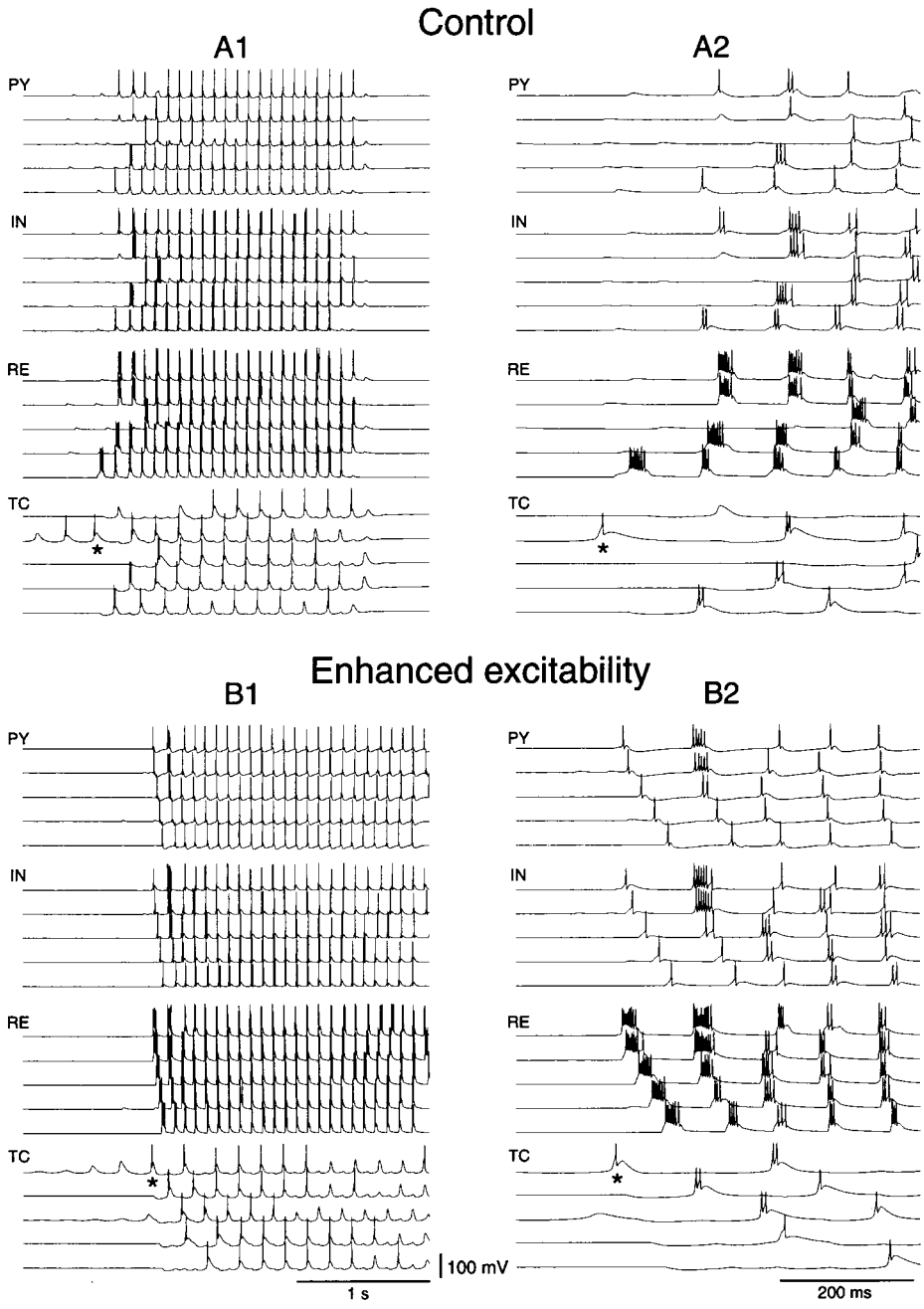

Fig. 5. Cellular patterns of oscillations in a thalamocortical network. The network had four layers of PY, IN, RE and TC cells as schematized in Fig. 3A. (A1) Spontaneous spindle oscillation in control conditions. Five cells of each type, equally spaced in the network, are shown with 0.5 ms time step. (A2) Detail of the initiation of the same spindle wave with five times higher temporal resolution. (B1) Spontaneous spindle oscillation with enhanced excitability of cortical pyramidal cells. Same parameters and description as in A, except that PY cells had a more depolarized resting membrane potential of −60 mV and a reduced I_M current. (B2) Same simulation at higher temporal resolution. In both cases, the oscillation initiated by the discharge of one or several TC cells (asterisks indicate an initiator TC cell). Synaptic conductances were 0.2 μS (TC→RE AMPA receptors), 0.2 μS (RE→RE $GABA_A$ receptors), 0.02 μS (RE→TC $GABA_A$ receptors), 0.04 μS (RE→TC $GABA_B$ receptors), 1.2 μS (TC→PY AMPA receptors), 0.4 μS (TC→IN AMPA receptors), 0.01 μS (PY→TC AMPA receptors), 1.2 μS (PY→RE AMPA receptors. All other synaptic conductances were identical to Fig. 4.

depended on the values of excitatory synaptic conductances as propagation is a direct consequence of the effectiveness of pyramidal-to-pyramidal EPSPs.

Effect of enhancing the excitability of cortical pyramidal cells

Next, the role of cortical excitability was

investigated at the level of the thalamocortical network. The thalamocortical network was identical to that introduced previously to model interactions between cortex and thalamus in the genesis of spindle oscillations.[19] In addition to the one-dimensional cortical network described above, the model included thalamic RE and TC cells. Each cell type was modeled by a single compartment comprising calcium- and voltage-dependent currents identified in these cells and which account for their intrinsic firing properties (Fig. 3B).

Thalamic cells and their connectivity were identical to a previous model of thalamic oscillations[22] based on experiments on ferret thalamic slices. TC and RE cells both generated low-threshold spikes due to the presence of a T-type calcium current (Fig. 3B) and TC cells had an additional inward current I_h which, in combination with I_T, generated intrinsic oscillatory behavior in TC cells. A calcium-dependent regulation of I_h accounted for the waxing and waning properties of oscillations. The model had two one-dimensional layers of 100 TC and 100 RE cells with each cell type contacting its 11 closest neighbors for each connection type. Intrinsic thalamic connectivity was mediated by AMPA receptors (TC → RE), a mixture of $GABA_A$ and $GABA_B$ receptors (RE → TC) and $GABA_A$ receptors (RE → RE).

The thalamocortical network thus comprised four one-dimensional layers (TC, RE, IN and PY) of 100 cells each (Fig. 3A). The connectivity between thalamic and cortical was more extended than intracortical and intrathalamic axonal projections, such as to contact 21 cells. These connections were mediated by AMPA receptors (TC → PY, TC → IN, PY → RE and PY → TC). More details on the network structure and biophysical models of ionic currents are given in Experimental Procedures and in a previous paper.[19]

This model included the hypothetical mechanism that cortical feedback produces dominant inhibitory postsynaptic potentials (IPSP) on TC cells, as explored in detail previously.[19] The "IPSP dominance" was implemented through strong corticothalamic EPSPs on RE cells, together with weaker direct EPSPs on TC cells. The resulting effect was that excitation of corticothalamic axons evoked a net inhibitory effect on TC cells, as observed experimentally *in vivo*.[1,16,42] The model established that this was the most optimal way for the cortex to recruit oscillations in the thalamus, because TC cells are powerfully recruited by IPSPs due to their rebound burst mechanisms.[19]

The behavior of such a network with 100 cells of each type is shown in Fig. 5. In control conditions, spindle oscillations started with the spontaneous firing of one or several TC cells (Fig. 5A). Several initiation sites occurred in the thalamus because of the heterogeneity of TC cells, as analysed previously.[19] Cortical initiation was also possible and was investigated in detail previously (see Fig. 9 in Ref. 19). The "initiator TC cells" of Fig. 5A (*) recruited the rest of the network through successive thalamus–cortex–thalamus recruitment loops, such that the oscillation generalized to the entire network within a few cycles. This model was shown to account for a number of different properties of barbiturate spindles, such as their patterns of initiation, synchrony and propagation following low-intensity cortical stimulation.[19]

The same simulation was performed with enhanced excitability of cortical pyramidal cells (Fig. 5B). As above, the augmentation of excitability was implemented through a decreased I_M conductance and a more depolarized level of −60 mV. In these conditions, the network displayed spindle oscillations with similar cellular characteristics as in control conditions. A marked difference, however, was that the oscillations invaded the extent of the network more rapidly, in about one cycle of the oscillation. This effect is clearly seen if local average membrane potentials of pyramidal cells are computed at equidistant sites (Fig. 6A and scheme). These average values reveal that in control conditions, the oscillation initiated almost simultaneously in two different sites (indicated by asterisks in Fig. 6A). With enhanced cortical excitability, the oscillation synchronized within a narrower time window.

The increased synchrony with enhanced cortical excitability was essentially due to the more depolarized resting level of PY cells. The contribution of the decreased I_M conductance was also significant, but less important in magnitude at the network level (not shown). The mechanism was that a substantial proportion of corticocortical and thalamocortical EPSPs in PY cells were subthreshold at a resting membrane potential of −70 mV and became suprathreshold at −60 mV, similarly to Fig. 4. The spontaneous firing of initiator TC cells initiated a fast-propagating discharge in the cortex (similar to Fig. 4A2) that in turn recruited the rest of thalamus into the oscillation. Consistent with this observation, suppressing PY → PY connections in the simulation of Fig. 5B led to similar initiation patterns as in Fig. 5A (not shown). Therefore, in the enhanced cortical excitability state, intracortical excitatory connections are more powerful, which results in a more compact network in which oscillations generalize more quickly.

For this mechanism to occur, it was important that the corticothalamic feedback acted through IPSP dominance on TC cells. If the discharge of pyramidal cells evoked too strong direct EPSPs on TC cells, the resulting shunt between cortical EPSPs and reticular IPSPs would not recruit oscillations in the TC cell, and the oscillations would remain local. If corticothalamic feedback mostly evoked IPSPs in TC cells, through discharging RE cells, then oscillations were efficiently evoked in the entire system

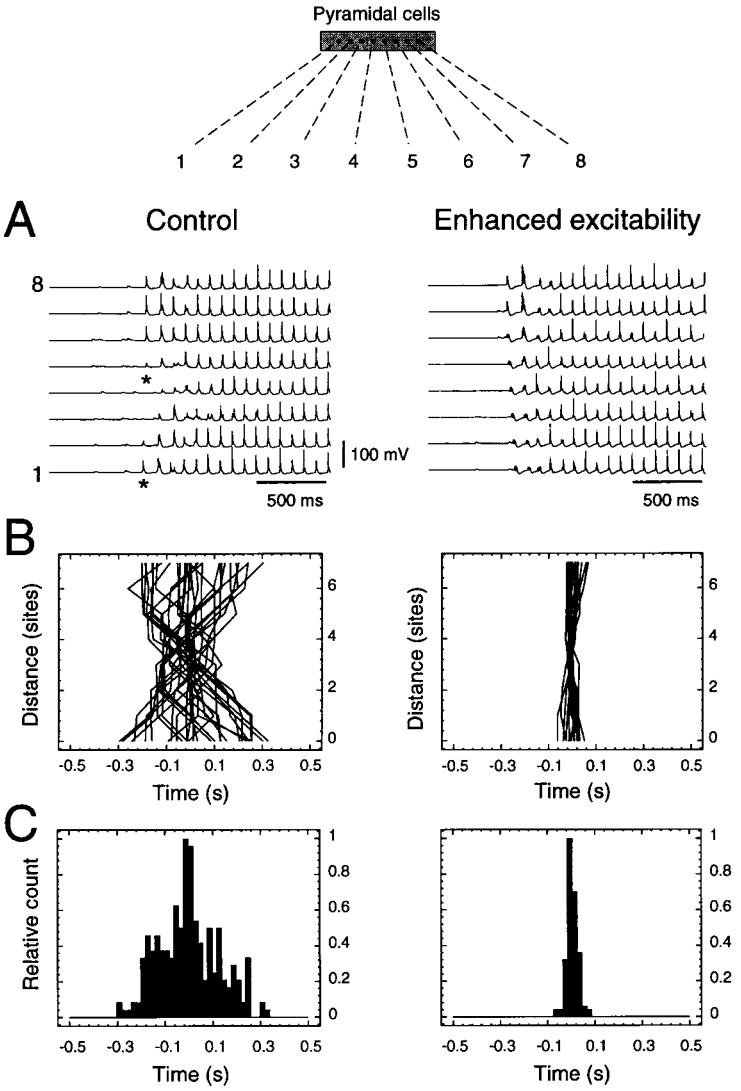

Fig. 6. Effect of enhancing cortical excitability on the spatiotemporal distribution of oscillations. Simulated spindle oscillations are shown for control conditions and when the excitability of cortical pyramidal cells was enhanced (left and right panels, respectively; simulations identical to Fig. 5). (A) Local average membrane potentials. 21 adjacent PY cells, taken at eight equally-spaced sites on the network (see scheme on top), were used to calculate each average. Asterisks indicate two simultaneous initiation sites. (B) Patterns of initiation. The onset of the oscillation was estimated from local averaged membrane potentials using the same procedure as in Fig. 1B. (C) Distribution of initiation times computed from B, similarly as in Fig. 1C.

through the rebound burst property of TC cells, similar to a mechanism described previously.[19]

Spatiotemporal coherence of simulated oscillations

To compare the model to experimental data, similar analyses as for LFPs were performed from the average local potentials of the model of Fig. 6A. Initiation times of simulated spindles were constructed from local averaged potentials, using the same criteria as for Fig. 1B. Spindle sequences ($n = 32$) were analysed in control conditions and initiated within time windows of 0.2 ± 0.1 s (Fig. 6B, left panel). These values were comparable to that obtained during barbiturate anesthesia and depressed cortex. Spindle sequences ($n = 20$) with enhanced cortical excitability initiated within time windows of about 0.06 ± 0.03 s (Fig. 6B, right panel), comparable to natural sleep spindles. The distribution of initiation times (Fig. 6C) also displayed standard deviation that were similar to experiments ($\sigma = 126$ ms and 24 ms for control and enhanced cortical excitability, respectively).

The similarity between the distribution of initiation times in the model and experiments (compare Fig. 1C with Fig. 6C), suggests that the intersite distance of 11 cells, used to calculate averages in the model, roughly corresponds to the interelectrode distance of 1 mm in the experiments. The propagation velocity of oscillations evoked by low-intensity

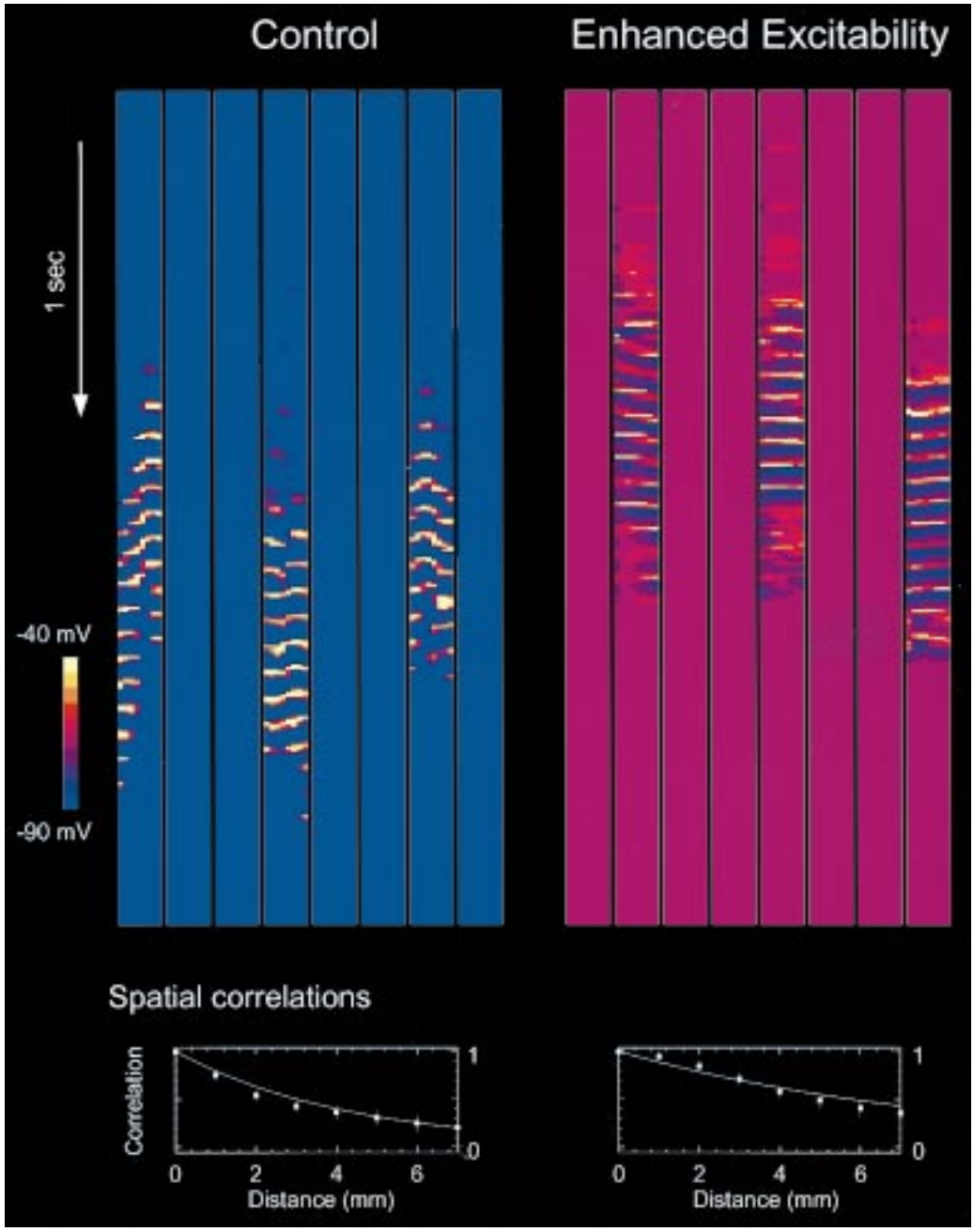

Fig. 7. Effect of enhancing cortical excitability on the spatiotemporal coherence of oscillations. Simulated spindle oscillations are shown for control conditions and for enhanced excitability of PY cells (left and right panels, respectively). (Top panels) Spatiotemporal maps of local averaged potentials. Maps were obtained from the simulations shown in Fig. 5, with time running from top to bottom (arrow of 1 s) in steps of 10 ms. In each column, the membrane potential is represented with a color scale ranging from − 90 mV or below (blue) to − 40 mV or above (yellow; see scale). (Bottom panels) Decay of correlations with distance, calculated from local averaged potentials. Spatiotemporal maps and correlations are displayed using the same procedures and scales as in Fig. 2.

cortical stimulation in experiments[14] is comparable to that of models using the same distance correspondence,[19] which indicates that the same model is consistent with both types of experiments, with one cell in the model representing about 315 neurons in the real cortex (see Experimental Procedures).

The effect of enhancing the excitability of cortical pyramidal cells on the coherence of oscillations is also apparent in spatiotemporal maps of the distribution of activity (Fig. 7). In control conditions, oscillatory activity began in one or two sites and progressively invaded the network (Fig. 7, left color panel). The oscillations had comparable synchrony and phase shifts as during barbiturate

anesthesia (compare with Fig. 2, Barbiturate). With enhanced cortical excitability, the simultaneity and synchrony of oscillations were enhanced, while phase shifts were reduced (Fig. 7C, right color panel).

The influence of cortical excitability on spatiotemporal coherence was also evidenced by calculating the decay of correlations with distance from local averaged potentials (Fig. 7, bottom panels). Spindles simulated in control conditions gave rise to correlation decay with a space constant of $\lambda = 4.36$ (in units of intersite distance). With enhanced cortical excitability, correlations stayed high for larger distances (space constant of $\lambda = 8.36$), although not as high as in natural sleep. However, similar to experiments, enhancing cortical excitability produced an increase of spatiotemporal coherence, as shown by a less steep correlation decay.

Effect of enhancing the excitability of different cell types

To compare the effect described above for pyramidal cells with that of other cell types, we have performed simulations in which the excitability of other cell types was altered. We tested whether similar results as above, obtained with enhanced pyramidal cell excitability (Fig. 8A), could also be obtained by changing the excitability of other cellular elements. The excitability of cortical interneurons was changed by using a more depolarized resting level, which enhanced the discharge following depolarizing inputs (Fig. 8B, left). However, this change had no significant effect at the network level (Fig. 8B, right). On the other hand, decreasing the excitability of interneurons, by using more hyperpolarized resting level, led to epileptic-like discharges (not shown). In this case, the disinhibited pyramidal cells fired strong discharges and entrained the network in a ~3 Hz oscillation, similar to the analysis of a previous model of spike-and-wave.[17] It is indeed known from experimental data that blocking $GABA_A$ receptors in cerebral cortex leads to spike-and-wave seizures at 2–3 Hz.[42a,43a]

Enhancing the excitability of thalamic cells was also investigated. In RE cells, the excitability was changed by using a smaller leak conductance, similar to the effect of noradrenaline on these cells.[35] This resulted in stronger burst discharges (Fig. 8C, left). In network simulations, enhancing the excitability of RE cells had a marked effect on oscillation frequency, as analysed previously,[17] but there was no prominent effect on the simultaneity and spatiotemporal coherence of oscillations (Fig. 8C, right). In TC cells, the excitability was enhanced by using smaller leak K^+ currents, mimicking the effect of acetylcholine and noradrenaline in these cells.[35] This resulted in lower burst threshold in response to hyperpolarizing current (Fig. 8D, left). At the network level, enhancing TC cell excitability led to significantly shorter spindle oscillations (not shown) but had no significant effect on spatiotemporal coherence (Fig. 8D, right).

These simulations indicate that the excitability of cortical pyramidal cells seems to be the most critical cellular parameter that affects the simultaneity and spatiotemporal coherence of oscillations generated by thalamocortical loops.

DISCUSSION

This report has presented a numerical analysis of multisite field potentials in cat cerebral cortex during synchronized spindle oscillations. A possible cellular mechanism was suggested to explain these results and this mechanism was tested using a computational model of corticothalamic interactions. We relate here these experimental results to previous studies, discuss the plausibility of the proposed cellular mechanism, and provide predictions to test the validity of this mechanism.

The spatiotemporal coherence of sleep spindle oscillations

Sleep spindles are a classical landmark of the onset of slow-wave sleep in the human EEG. In cats, sleep spindles are a prominent feature of the onset of slow-wave sleep and also are the most prominent manifestation in the EEG during barbiturate anesthesia. These “barbiturate spindles” have the same cellular features as natural sleep spindles, namely they are generated in thalamic circuits following complex interactions involving RE and TC cells.[47,48,55]

In the human EEG as well as in barbiturate-anesthetized animals, spindle oscillations appear nearly simultaneously in both hemispheres. The coherence of spindle oscillations has been re-examined here, by comparing three different states: natural sleep, barbiturate anesthesia and natural sleep with depressed cortex. In all cases, oscillations appeared nearly simultaneously in neighboring recording electrodes in the cortex. However, at closer scrutiny, systematic differences were apparent. This paper provided a quantification of the spatiotemporal distribution of electrical activity across the cortex, the patterns of initiation and the decay of correlations with distance. It appeared that oscillations may manifest different degree of spatiotemporal coherence in the cortex: the remarkable synchrony during natural sleep contrasts with the variability of initiation patterns during barbiturate anesthesia or natural sleep with depressed cortex.

Early studies with multiple electrodes *in vivo*[53,54] showed spindle oscillations initiating at different times, suggesting that they were propagating across the network. In contrast, our results do not show systematic propagation (Fig. 1A). During the less

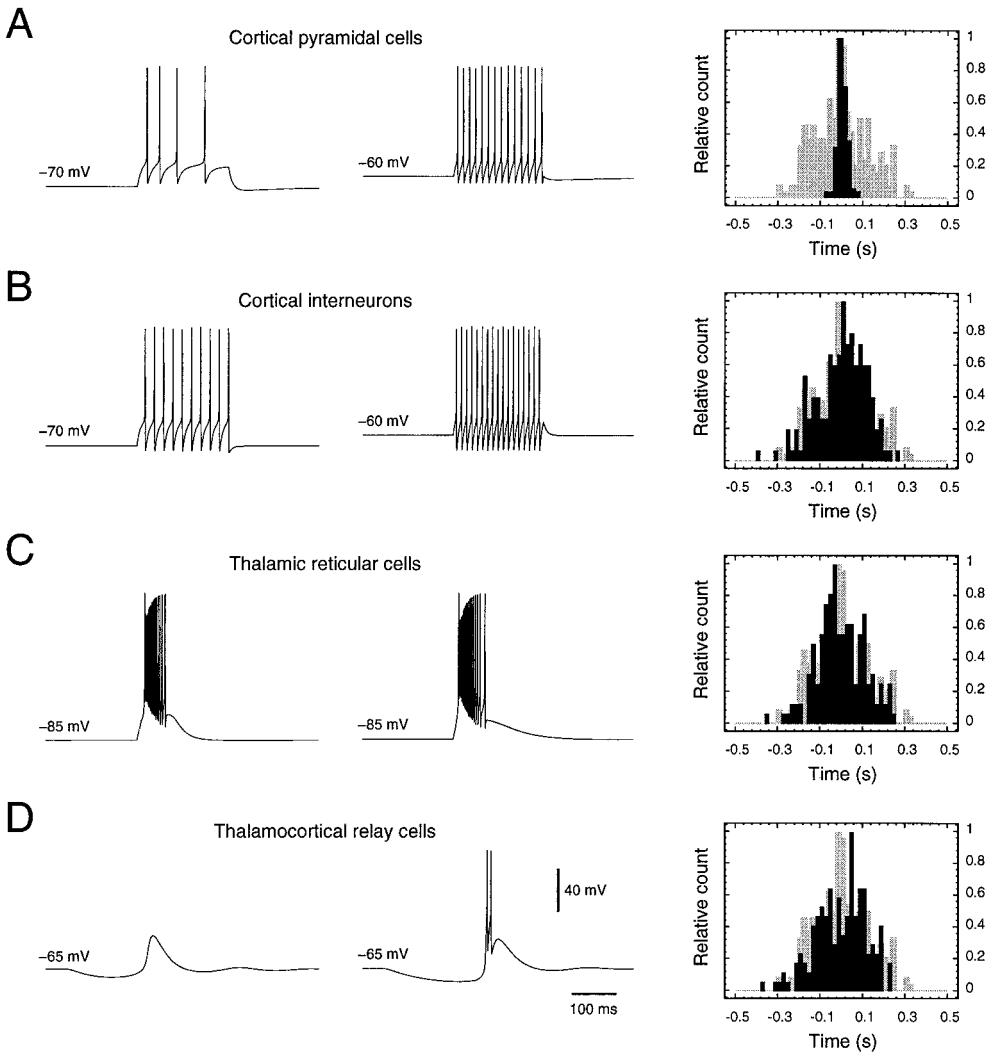

Fig. 8. Effect of enhancing the excitability of different cell types. Simulations were run in which all cell types were identical to the control simulation of Fig. 5A, except that one cell type had enhanced excitability. For each cell type, the left panels show the effect of enhancing excitability on the discharge of the cell, and the right panel shows its effect at the network level by showing the distribution of initiation times obtained for 20 simulated spindle sequences. (A) Enhancing the excitability of PY cells (lower I_M conductance, from 0.07 to 0.02 mS/cm^2, and lower resting level, from −70 to −60 mV) had an effect both on cellular response (left; current pulse of 0.75 nA during 200 ms) and on network behavior (right; same simulations as shown in Fig. 6). (B) Enhancing the excitability of IN cells (lower resting level, from −70 to −60 mV) had an effect on cellular discharges (left; current pulse of 0.5 nA during 200 ms) but not on network behavior (right). (C) Enhancing the excitability of RE cells (lower leak conductance, from 0.05 mS/cm^2 to 0.02 mS/cm^2) affected burst responses (left; current pulse of 0.3 nA during 10 ms) but network behavior was minimally affected (right). (D) Enhancing the excitability of TC cells (lower leak K^+ conductance, from 3 nS to 1 nS) affected burst threshold (hyperpolarizing current pulse of −0.03 nA during 200 ms) but had little effect on network behavior. All histograms shown in light grey correspond to the control simulation of Fig. 6C.

coherent state, initiation patterns show differences of one to three cycles of the oscillation, revealing propagating patterns at neighboring sites within time windows of less than 500 ms (see electrodes 1 to 5 in Fig. 1A, Barbiturate anesthesia). However, these propagating patterns were local in both time and space and the oscillations came quickly (less than 500 ms) to a state where the entire system oscillated in unison. These results are in accordance with earlier studies in cats during barbiturate anesthesia, showing high variability in the patterns of oscillations, with local propagation and large-scale synchrony over large cortical territories.[4] Our *in vivo* recordings contrast with thalamic slices showing systematic propagation.[30] Computational models showed that systematic propagating patterns in isolated thalamic circuits are indeed compatible with more simultaneous patterns in intact thalamocortical circuits.[19]

During natural sleep, by contrast with barbiturate spindles, the initiation patterns of oscillations are much more strict and less variable (Fig. 1B), the

spatiotemporal coherence is enhanced (Fig. 2, top) and correlations decay less steeply with distance (Fig. 2, bottom). These features show that natural sleep oscillations represent a state of enhanced large-scale synchrony compared to barbiturate spindles. Interestingly, artificial depression of the cortex during natural sleep leads to similar patterns of large-scale synchrony as during barbiturate anesthesia (Figs. 1 and 2). This indicates that the underlying mechanism must involve cortical cells, contrary to the exclusively intrathalamic synchronizing mechanisms proposed by Andersen and Andersson.[3]

A cellular mechanism for large-scale synchrony

How can changes in the cortex affect the synchrony of thalamic-generated oscillations with no change in the thalamus? The hypothesis explored by the model is that this effect could be due to a change in the excitability of cortical cells, acting on the thalamus through corticothalamic feedback projections.

The first component in this mechanism is the nature of corticothalamic feedback. *In vivo* recordings consistently show that the cortex is very effective in recruiting oscillations in the thalamus.[14,42,50] In models, this feature could be obtained only if cortical EPSPs were very effective on RE cells and had less direct effect on TC cells.[19] Consistent with this, intracellular recordings of TC cells *in vivo* consistently showed dominant IPSPs in TC cells following cortical stimulation[1,16,42] while lesioning the RE nucleus revealed EPSPs in TC cells.[16] Modeling studies established that this property of "IPSP dominance" in TC cells is the most optimal way for the cortex to recruit oscillations in the thalamus.[19]

The second component is the role of cortical excitability. Depressing cortical responsiveness, either by using extracellular potassium or with barbiturates, increases the threshold EPSP needed to fire pyramidal cells. Consequently, an oscillation would need several cycles to invade the entire network, as several successive cortex–thalamus–cortex recruitment loops are necessary before the network oscillates in unison (Fig. 6; Fig. 7, Control). In a more responsive cortex, with more depolarized pyramidal cells, a significant proportion of subthreshold EPSPs became suprathreshold. The consequence was that the more excitable cortex generated fast-propagating discharges, providing a very coherent feedback onto the thalamus, and generating highly synchronized oscillations in the entire system (Fig. 6; Fig. 7, Enhanced excitability).

This mechanism is consistent with the available data suggesting a great difference of excitability during natural sleep and barbiturate anesthesia. First, the discharge rate of cortical pyramidal cells is greatly reduced with barbiturates, proportional to the depth of anesthesia[31] whereas natural sleep is characterized by a similar average discharge rate as the awake state.[24,46] Second, the early phases of natural sleep, during which most spindles occur, are still characterized by a relatively high level of discharge of activating systems from brainstem, basal forebrain and posterior hypothalamus.[43] Third, intracellular recordings of cortical pyramidal cells show that the resting level of the membrane is significantly lower during barbiturate anesthesia (-70 to -80 mV in Ref. 49), compared to the depolarized level following stimulation of activating systems (about -60 mV in Ref. 44).

The present model described an effect on large-scale synchrony similar to the effect seen in experiments over distances of about 7 mm in cerebral cortex. Can similar mechanisms apply to larger cortical distances? An attracting possibility would be that EPSPs from the rostral intralaminar thalamic neurons become suprathreshold when pyramidal cells have a more depolarized resting level, leading to enhanced large-scale synchrony. Thalamic intralaminar neurons project over widespread neocortical areas and tend to contact cortical neurons distally in layer I.[29] It was proposed that intralaminar neurons play an important role in co-ordinating oscillations over the entire cortical mantle.[34,41] The observation that these neurons discharge robust spike bursts within each cycle of spindle oscillations[45] suggests that they may also play a significant role in co-ordinating the coherence of spindles. We suggest that cortical pyramidal cells are sensitive to intralaminar EPSPs only when they are in a more excitable state, with resting level around -60 mV, leading to synchrony that extends over wide cortical territories. More information about the electrophysiological properties and connectivity of intralaminar cells would be needed to investigate this hypothesis further.

Predictions

The first prediction provided by the model is that the excitability of cortical cells greatly affects the spread of discharges (Fig. 4). It is known that in neocortical slices, local stimulation of the white matter produces limited horizontal propagation,[2,9,15] but the application of $GABA_A$ antagonists generates epileptic discharges which propagate very efficiently in the horizontal direction.[2,9] We suggest that, in addition to $GABA_A$ antagonists, horizontal propagation should be markedly enhanced in cortical slices by using extracellular application of neuromodulators, such as acetylcholine or noradrenaline, through an increase of excitability of cortical pyramidal cells. The velocity of these fast-propagating discharges (100–200 mm/s) depends on the level of excitability (Fig. 4B) and therefore should be dependent on the neuromodulator concentration. At the level of the thalamocortical system, fast-propagating cortical discharges should also be detectable by high-resolution optical recording methods *in vivo*.

Second, the model predicts that natural sleep and barbiturate anesthesia correspond to different levels of resting membrane potential in cortical pyramidal cells. If intracellular recordings could be performed in neocortical pyramidal cells during natural sleep, the model predicts that it should reveal a relatively depolarized resting level, close to −60 mV, compared to the hyperpolarized resting level of −70 mV to −80 mV typical of barbiturate anesthesia.

Third, propagating oscillatory waves may be different during natural sleep. It was shown that during barbiturate anesthesia, low-intensity electrical stimulation of the cortex can induce propagating oscillatory waves.[14] These propagating oscillations resisted cortical transection,[14] suggesting little involvement of horizontal intracortical connections. The present model suggests that, contrary to these barbiturate spindles, intracortical connections should have a critical role in the simultaneity of natural sleep spindles. This directly predicts that, during natural sleep, propagating oscillations evoked by cortical stimulation should not occur. A corollary prediction is that cortical transection should affect the spatiotemporal patterns and synchrony of natural sleep spindle oscillations. This is supported by the observation of diminished interhemispheric synchrony of spindles following callosal transection.[7]

CONCLUSIONS

These experiments and models are compatible with a powerful role for the cortex in triggering and synchronizing oscillations generated in the thalamus, through corticothalamic feedback projections. The model suggests that intracortical mechanisms may be responsible for synchronizing oscillations over cortical distances of several millimeters through cortex–thalamus–cortex loops, thus providing a possible cellular mechanism to explain the genesis of large-scale coherent oscillations in the thalamocortical system.

Acknowledgements—Research supported by Medical Research Council of Canada, Human Science Frontier Program and Fonds de la Recherche en Santé du Québec. D.C. was supported by a Savoy Foundation studentship.

REFERENCES

1. Ahlsen G., Grant K. and Lindstrom S. (1982) Monosynaptic excitation of principal cells in the lateral geniculate nucleus by corticofugal fibers. *Brain Res.* **234,** 454–458.
2. Albowitz B. and Kuhnt U. (1993) The contribution of intracortical connections to horizontal spread of activity in the neocortex as revealed by voltage sensitive dyes and a fast optical recording method. *Eur. J. Neurosci.* **5,** 1349–1359.
3. Andersen P. and Andersson S. A. (1968) *Physiological Basis of the Alpha Rhythm.* Appleton Century Crofts, New York.
4. Andersen P., Andersson S. A. and Lomo T. (1967) Nature of thalamo-cortical relations during spontaneous barbiturate spindle activity. *J. Physiol.* **192,** 283–307.
6. Baranyi A., Szente M. B. and Woody C. D. (1993) Electrophysiological characterization of different types of neurons recorded *in vivo* in the motor cortex of the cat. II. Membrane parameters, action potentials, current-induced voltage responses and electrotonic structures. *J. Neurophysiol.* **69,** 1865–1879.
7. Bremer F., Brihaye J. and André-Balisaux G. (1956) Physiologie et pathologie du corps calleux. *Schweiz. Arch. Neurol. Psychiat.* **78,** 31–87.
8. Bullock T. H. and McClune M. C. (1989) Lateral coherence of the electrocorticogram: a new measure of brain synchrony. *Electroenceph. clin. Neurophysiol.* **73,** 479–498.
9. Chagnac-Amitai Y. and Connors B. W. (1989) Horizontal spread of synchronized activity in neocortex and its control by GABA-mediated inhibition. *J. Neurophysiol.* **61,** 747–758.
10. Connors B. W. and Gutnick M. J. (1990) Intrinsic firing patterns of diverse neocortical neurons. *Trends Neurosci.* **13,** 99–104.
11. Connors B. W., Gutnick M. J. and Prince D. A. (1982) Electrophysiological properties of neocortical neurons *in vitro*. *J. Neurophysiol.* **48,** 1302–1320.
12. Contreras D., Destexhe A. and Steriade M. (1997) Spindle oscillations during cortical spreading depression in naturally sleeping cats. *Neuroscience* **77,** 933–936.
13. Contreras D., Destexhe A., Sejnowski T. J. and Steriade M. (1996) Control of spatiotemporal coherence of a thalamic oscillation by corticothalamic feedback. *Science* **274,** 771–774.
14. Contreras D., Destexhe A., Sejnowski T. J. and Steriade M. (1997) Spatiotemporal patterns of spindle oscillations in cortex and thalamus. *J. Neurosci.* **17,** 1179–1196.
15. Contreras D., Sugimori M. and Llinás R. (1997) Afferent stimulation frequency determines spatial distribution of excitation in neocortex. A voltage-sensitive dye study. *Soc. Neurosci. Abstr.* **23,** 1005.
16. Deschênes M. and Hu B. (1990) Electrophysiology and pharmacology of the corticothalamic input to lateral thalamic nuclei: an intracellular study in the cat. *Eur. J. Neurosci.* **2,** 140–152.
17. Destexhe A. (1998) Spike-and-wave oscillations based on the properties of $GABA_B$ receptors. *J. Neurosci.* **18,** 9099–9111.
18. Destexhe A. and Sejnowski T. J. (2000) *The Thalamocortical Assembly*. Oxford University Press, Oxford, U.K. (in press).
19. Destexhe A., Contreras D. and Steriade M. (1998) Mechanisms underlying the synchronizing action of corticothalamic feedback through inhibition of thalamic relay cells. *J. Neurophysiol.* **79,** 999–1016.
20. Destexhe A., Mainen Z. F. and Sejnowski T. J. (1998) Kinetic models of synaptic transmission. In *Methods in Neuronal Modeling* (eds Koch C. and Segev I.), 2nd edn, pp. 1–26. MIT, Cambridge, MA.
21. Destexhe A., McCormick D. A. and Sejnowski T. J. (1993) A model for 8–10 Hz spindling in interconnected thalamic relay and reticularis neurons. *Biophys. J.* **65,** 2474–2478.
22. Destexhe A., Bal T., McCormick D. A. and Sejnowski T. J. (1996) Ionic mechanisms underlying synchronized oscillations and propagating waves in a model of ferret thalamic slices. *J. Neurophysiol.* **76,** 2049–2070.

23. Destexhe A., Contreras D., Steriade M., Sejnowski T. J. and Huguenard J. R. (1996) *In vivo, in vitro* and computational analysis of dendritic calcium currents in thalamic reticular neurons. *J. Neurosci.* **16,** 169–185.
24. Evarts E. V. (1964) Temporal patterns of discharge of pyramidal tract neurons during sleep and waking in the monkey. *J. Neurophysiol.* **27,** 152–171.
25. Hersch S. M. and White E. L. (1981) Thalamocortical synapses on corticothalamic projections neurons in mouse SmI cortex: electron microscopic demonstration of a monosynaptic feedback loop. *Neurosci. Lett.* **24,** 207–210.
26. Hines M. L. and Carnevale N. T. (1997) The NEURON simulation environment. *Neural Computation* **9,** 1179–1209.
27. Hodgkin A. L. and Huxley A. F. (1952) A quantitative description of membrane current and its application to conduction and excitation in nerve. *J. Physiol.* **117,** 500–544.
28. Huguenard J. R. and Prince D. A. (1992) A novel T-type current underlies prolonged calcium-dependent burst firing in GABAergic neurons of rat thalamic reticular nucleus. *J. Neurosci.* **12,** 3804–3817.
29. Jones E. G. (1985) *The Thalamus.* Plenum, New York.
30. Kim U., Bal T. and McCormick D. A. (1995) Spindle waves are propagating synchronized oscillations in the ferret LGNd *in vitro*. *J. Neurophysiol.* **74,** 1301–1323.
31. Kostopoulos G., Gloor P., Pellegrini A. and Gotman J. (1981) A study of the transition from spindles to spike and wave discharge in feline generalized penicillin epilepsy: microphysiological features. *Expl Neurol.* **73,** 55–77.
32. Krnjevic K., Pumain R. and Renaud L. (1971) The mechanism of excitation by acetylcholine in the cerebral cortex. *J. Physiol.* **215,** 247–268.
33. Landry P. and Deschênes M. (1981) Intracortical arborizations and receptive fields of identified ventrobasal thalamocortical afferents to the primary somatic sensory cortex in the cat. *J. comp. Neurol.* **199,** 345–371.
34. Llinás R., Ribary U., Joliot M. and Wang X. J. (1994) Content and context in temporal thalamocortical binding. In *Temporal Coding in the Brain* (eds Buzsaki G., Llinás R., Singer W., Berthoz A. and Christen Y.), pp. 251–272. Springer, Berlin.
35. McCormick D. A. (1992) Neurotransmitter actions in the thalamus and cerebral cortex and their role in neuromodulation of thalamocortical activity. *Prog. Neurobiol.* **39,** 337–388.
36. McCormick D. A. and Prince D. A. (1986) Mechanisms of action of acetylcholine in the guinea-pig cerebral cortex *in vitro*. *J. Physiol.* **375,** 169–194.
37. McCormick D. A. and Williamson A. (1989) Convergence and divergence of neurotransmitter action in human cerebral cortex. *Proc. natn. Acad. Sci. U.S.A.* **86,** 8098–8102.
38. McCormick D. A., Wang Z. and Huguenard J. (1993) Neurotransmitter control of neocortical neuronal activity and excitability. *Cerebral Cortex* **3,** 387–398.
39. Press W. H., Flannery B. P., Teukolsky S. A. and Vetterling W. T. (1986) *Numerical Recipes. The Art of Scientific Computing*. Cambridge University Press, Cambridge, U.K.
40. Rausell E. and Jones E. G. (1995) Extent of intracortical arborization of thalamocortical axons as a determinant of representational plasticity in monkey somatic sensory cortex. *J. Neurosci.* **15,** 4270–4288.
41. Ribary U., Ioannides A. A., Singh K. D., Hasson R., Bolton J. P., Lado F., Mogilner A. and Llinás R. (1991) Magnetic field tomography of coherent thalamocortical 40-Hz oscillations in humans. *Proc. natn. Acad. Sci. U.S.A.* **88,** 11037–11041.
42. Roy J. P., Clercq M., Steriade M. and Deschênes M. (1984) Electrophysiology of neurons in lateral thalamic nuclei in cat: mechanisms of long-lasting hyperpolarizations. *J. Neurophysiol.* **51,** 1220–1235.
42a. Steriade M. and Contreras D. (1998) Spike–wave complexes and fast components of cortically generated seizures. I. Role of neocortex and thalamus. *J. Neurophysiol* **80,** 1438–1455.
43. Steriade M. and McCarley R. W. (1990) *Brainstem Control of Wakefulness and Sleep*. Plenum, New York.
43a. Steriade M., Amzica F., Neckelmann D. and Timofeev I. (1998) Spike–wave complexes and fast components of cortically generated seizures. II. Extra- and intracellular patterns. *J. Neurophysiol* **80,** 1456–1479.
44. Steriade M., Amzica F. and Nuñez A. (1993) Cholinergic and noradrenergic modulation of the slow (∼0.3 Hz) oscillation in neocortical cells. *J. Neurophysiol.* **70,** 1384–1400.
45. Steriade M., Curro Dossi R. and Contreras D. (1993) Electrophysiological properties of intralaminar thalamocortical cells discharging rhythmic (approximately 40 Hz) spike-bursts at approximately 1000 Hz during waking and rapid eye movement sleep. *Neuroscience* **56,** 1–9.
46. Steriade M., Deschênes M. and Oakson G. (1974) Inhibitory processes and interneuronal apparatus in motor cortex during sleep and waking. I. Background firing and responsiveness of pyramidal tract neurons and interneurons. *J. Neurophysiol.* **37,** 1065–1092.
47. Steriade M., Jones E. G. and Llinás R. R. (1990) *Thalamic Oscillations and Signalling.* John Wiley and Sons, New York.
48. Steriade M., McCormick D. A. and Sejnowski T. J. (1993) Thalamocortical oscillations in the sleeping and aroused brain. *Science* **262,** 679–685.
49. Steriade M., Nuñez A. and Amzica F. (1993) A novel slow (<1 Hz) oscillation of neocortical neurons *in vivo*: depolarizing and hyperpolarizing components. *J. Neurosci.* **13,** 3252–3265.
50. Steriade M., Wyzinski P. and Apostol V. (1972) Corticofugal projections governing rhythmic thalamic activity. In *Corticothalamic Projections and Sensorimotor Activities* (eds Frigyesi T. L., Rinvik E. and Yahr M. D.), pp. 221–272. Raven, New York.
51. Thompson S. M. (1994) Modulation of inhibitory synaptic transmission in the hippocampus. *Prog. Neurobiol.* **42,** 575–609.
52. Traub R. D. and Miles R. (1991) *Neuronal Networks of the Hippocampus.* Cambridge University Press, Cambridge, U.K.
53. Verzeano M. and Negishi K. (1960) Neuronal activity in cortical and thalamic networks. A study with multiple microelectrodes. *J. gen. Physiol.* **43,** 177–195.
54. Verzeano M., Laufer M., Spear P. and McDonald S. (1965) L'activité des réseaux neuroniques dans le thalamus du singe. *Actualités Neurophysiologiques* **6,** 223–251.
55. von Krosigk M., Bal T. and McCormick D. A. (1993) Cellular mechanisms of a synchronized oscillation in the thalamus. *Science* **261,** 361–364.
56. Wang Z. and McCormick D. A. (1993) Control of firing mode of corticotectal and corticopontine layer V burst-generating neurons by norepinephrine, acetylcholine, and 1S,3R-ACPD. *J. Neurosci.* **13,** 2199–2216.
57. White E. L. and Hersch S. M. (1982) A quantitative study of thalamocortical and other synapses involving the apical dendrites of corticothalamic cells in mouse SmI cortex. *J. Neurocytol.* **11,** 137–157.

(*Accepted* 11 *January* 1999)